NANO LETTERS

Letter

pubs.acs.org/NanoLett

Giant-Amplitude, High-Work Density Microactuators with Phase Transition Activated Nanolayer Bimorphs

Kai Liu,[†,‡] Chun Cheng,[†] Zhenting Cheng,[§] Kevin Wang,[†,‡] Ramamoorthy Ramesh,[†,‡] and Junqiao Wu*[,†,‡]

[†]Department of Materials Science and Engineering, University of California, Berkeley, California 94720, United States

[‡]Materials Sciences Division, Lawrence Berkeley National Laboratory, Berkeley, California 94720, United States

[§]Department of Electrical Engineering and Computer Sciences, University of California, Berkeley, California 94720, United States

Supporting Information

ABSTRACT: Various mechanisms are currently exploited to transduce a wide range of stimulating sources into mechanical motion. At the microscale, simultaneously high amplitude, high work output, and high speed in actuation are hindered by limitations of these actuation mechanisms. Here we demonstrate a set of microactuators fabricated by a simple microfabrication process, showing simultaneously high performance by these metrics, operated on the structural phase transition in vanadium dioxide responding to diverse stimuli of heat, electric current, and light. In both ambient and aqueous conditions, the actuators bend with exceedingly high displacement-to-length ratios up to 1 in the sub-100 μm length scale, work densities over 0.63 J/cm^3, and at frequencies up to 6 kHz. The functionalities of actuation can be further enriched with integrated designs of planar as well as three-dimensional geometries. Combining the superior performance, high durability, diversity in responsive stimuli, versatile working environments, and microscale manufacturability, these actuators offer potential applications in microelectromechanical systems, microfluidics, robotics, drug delivery, and artificial muscles.

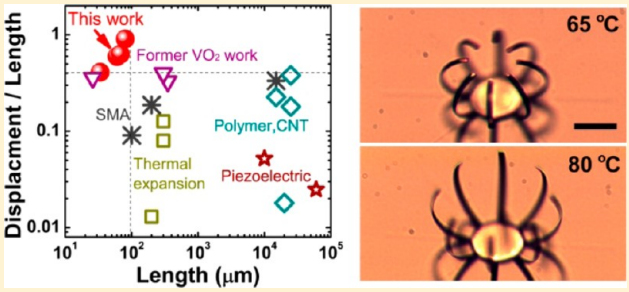

KEYWORDS: *Vanadium dioxide, phase transition, bimorph, actuator, microfabrication*

Direct conversion of external stimuli to mechanical motion at the micro- to nanoscale is of vital importance in advanced technologies including micro- and nanoelectromechanical systems, microrobotics, and biomimetics.[1−3] A wide range of materials featuring different stimuli-responsive properties are used for the actuation. On the inorganic side, differential thermal expansion,[4−6] piezoelectric ceramics,[7−10] and shape memory alloys (SMAs)[11,12] are typically utilized. The relative size change (strain) in these systems is usually low (except for SMAs), on the order of 10^{-4}∼10^{-3} even at strong stimuli such as high operating voltage or large temperature change. Consequently, they typically output small displacements far shorter than the actuator length, even with magnification mechanisms such as assembled in a bimorph structure. Actuators based on polymers or carbon nanotubes exhibit high flexibility and huge size change,[1,13−17] but their intrinsically low response speed, weak force output, and incompatibility with current microfabrication processes present severe limitations. Therefore, it is much desired to develop microactuators that can deliver simultaneously high amplitude and strong force at high speed by using conventional microfabrication techniques.

The fundamental reason that high amplitude and high force tend to be mutually exclusive is related to the limited output work density. The volumetric work density describes maximum mechanical work output per unit volume of active material that drives the actuation. It is given by $E{\cdot}\varepsilon^2/2$, where E is the Young's modulus of the active material, which determines the strength of force, and ε is the maximum strain, which limits the actuation amplitude.[1] Figure 1a shows the E versus ε plot of a range of active materials for actuation,[1,18,19] in comparison to vanadium dioxide (VO_2), the material we used in this work. It can be seen that owing to its simultaneously high E (∼140 GPa) and high ε (∼ 1% in single crystals), a work density as high as 7 J/cm^3 is theoretically possible by using VO_2 as the driving material. This is comparable to SMAs, over an order of magnitude higher than that of inorganic materials and electrostrictive polymers, and 3 orders of magnitude higher than human muscles (∼ 0.008 J/cm^3).[1] On the other hand, although being able to deliver high work densities, SMAs need a wide temperature variation for reactivation in cyclic actuation; moreover, when thickness is reduced to the submicrometer scale, SMAs tend to lose the memory function owing to martensite-austenite phase compatibility issues. As a result,

Received: September 12, 2012
Revised: November 13, 2012
Published: November 16, 2012

   dx.doi.org/10.1021/nl303405g | *Nano Lett.* 2012, 12, 6302−6308

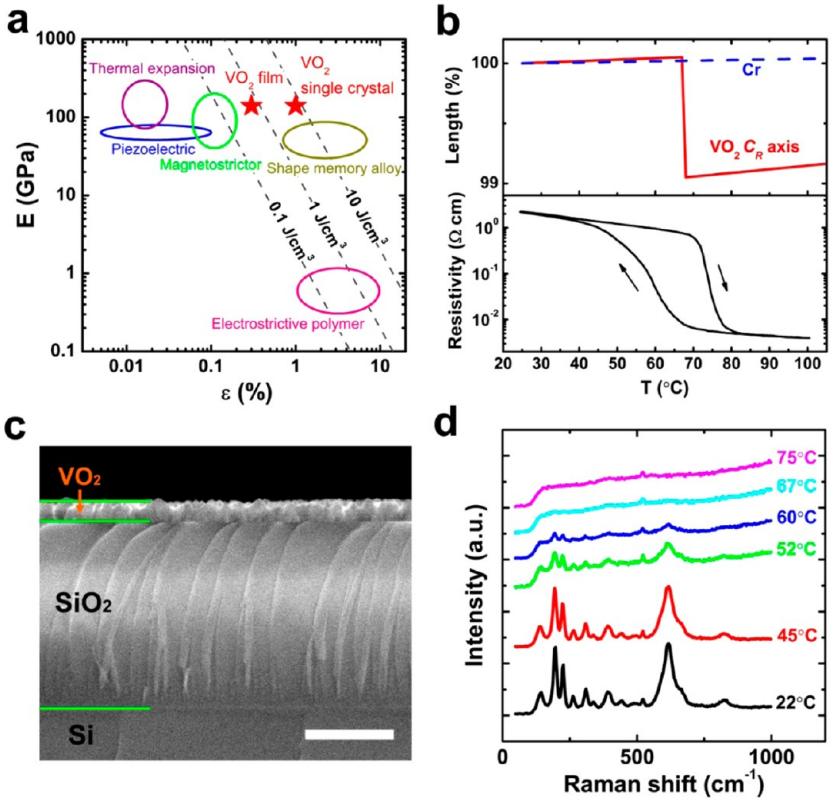

Figure 1. Properties of VO_2 thin films prepared. (a) Young's modulus (E) versus strain (ε) plot of various actuation materials. Data for high-strain piezoelectric ceramics, thermal expansion (ΔT = 10 K), magnetostrictor, shape memory alloys, and electrostrictive polymers are summarized from refs 1, 18, and 19. Also plotted are the contours of equal volumetric work density calculated using $E{\cdot}\varepsilon^2/2$. (b) Upper panel: Schematic plot of the transformation strain and thermal expansion of VO_2 and Cr. Lower panel: Temperature-dependent resistivity of a VO_2 film measured by four-probe method, showing the metal–insulator phase transition. (c) Cross-sectional SEM image of a VO_2 film deposited on SiO_2/Si substrate. The scale bar is 500 nm. (d) Raman spectra of a VO_2 thin film at different temperatures. Note that the small peak at 520 cm^{-1} is from the Si substrate.

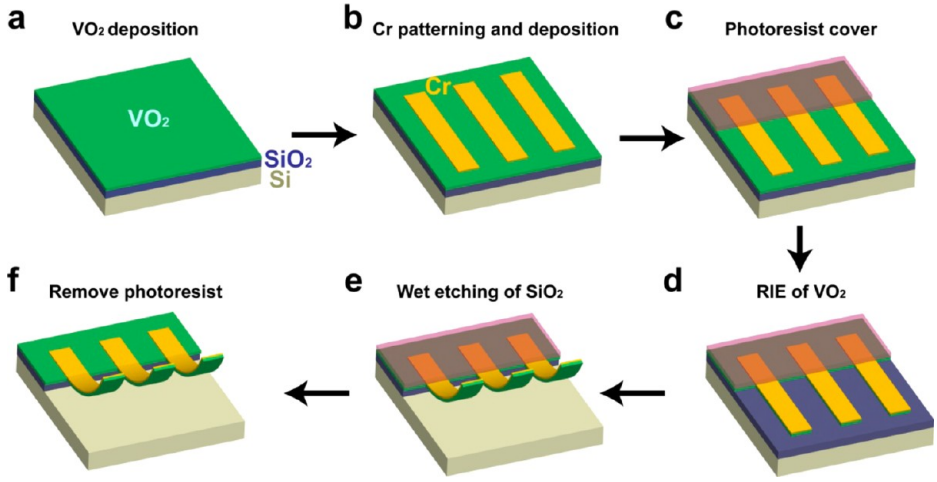

Figure 2. Schematic of microfabrication process. (a) Pulsed laser depositing VO_2 thin film on SiO_2/Si substrate. (b) Defining, depositing, and annealing the Cr pattern. (c) Partially covering the pattern with photoresist. (d) Dry etching the exposed VO_2 film. (e) BOE etching SiO_2 layer exposed and under the Cr/VO_2 pattern. (f) Dissolving the photoresist by replacing BOE gradually with water and then acetone.

SMA actuators are currently limited to low operating frequencies and low displacement-to-length ratios.[11,18]

VO_2 undergoes a thermally driven metal–insulator phase transition (MIT) accompanied by a structural transition slightly above room temperature (67 °C).[20−22] As its lattice changes from monoclinic (insulating, I) to rutile (metallic, M) structure upon heating across the MIT, VO_2 shrinks by a transformation strain of $\varepsilon \sim 1\%$ along the c-axis of the rutile phase (c_R) (Figure 1b), while expanding along the other two directions.[21] Combining the high E which is expected for a transition metal oxide, the high ε, the low stimulating temperature needed, the intrinsically fast MIT process (~ picosecond),[23] VO_2 arises as an ideal driving material for microscale actuation. Indeed, bimorphs of Cr on VO_2 nanowires[24] and VO_2 film on Si cantilevers[25,26] have been reported showing high bending amplitudes under direct heating; however, devices in these

dx.doi.org/10.1021/nl303405g | Nano Lett. 2012, 12, 6302−6308

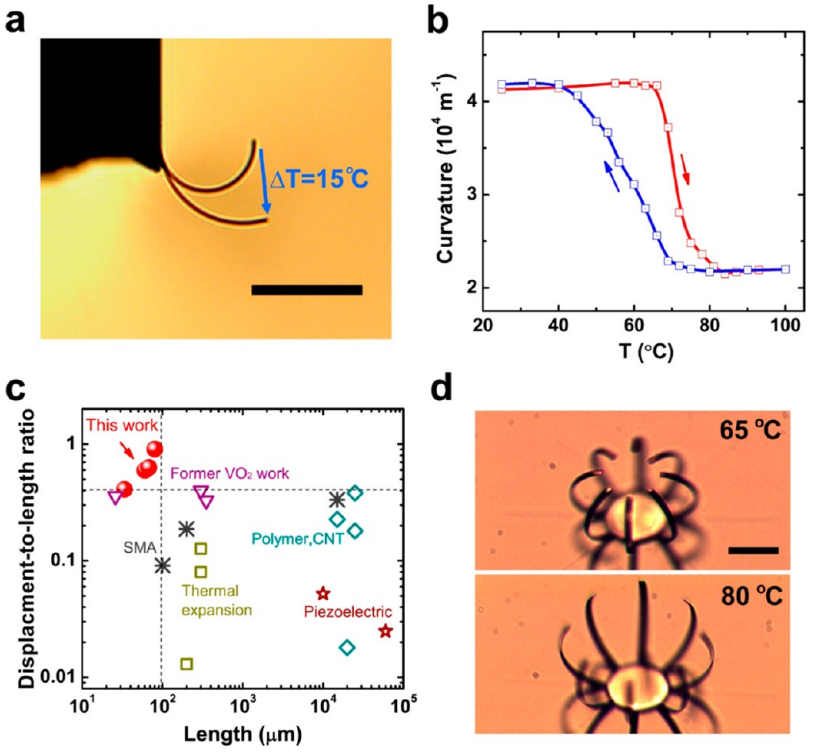

Figure 3. Thermally activated bimorph microactuators. (a) A cantilevered bimorph showing a large bending amplitude when temperature is increased by ΔT = 15 °C. The scale bar is 50 μm. (b) Dependence of bimorph curvature on temperature across the VO_2 phase transition (bimorph is Cr/VO_2 = 50/118 nm, annealed at 200 °C). (c) Ratio of actuation amplitude (tip displacement) to actuator length D/L, compared to that of thermal bimorphs (refs 4−6), piezoelectric bimorphs (refs 7, 10), shape memory alloy-based bimorphs (refs 11, 12), polymer or CNTs (refs 13−16), and other VO_2 nanowires or films based bimorphs (refs 24−26). (d) Microactuator with a "palm" structure, showing the fingers closed at 65 °C and open at 80 °C. The scale bar is 50 μm.

approaches cannot be lithographically fabricated to achieve different geometries and functionalities for fitting various microactuation needs, and the observed speeds (~ 300 Hz) and amplitudes were far from the theoretical limits.

In this work, we demonstrate a set of Cr/VO_2 bimorph microactuators with layers in nanoscale thicknesses using batch microfabrication, and the devices exhibit superior performance by nearly all metrics. In addition to the high work density output and high response speed expected, they offer the highest displacement-to-length ratio in the sub-100 μm length scale. They respond with high sensitivities to various thermal, electrothermal, and photothermal stimuli and work with high durability in both ambient and aqueous conditions.

The microactuators were fabricated by patterning and etching Cr/VO_2 double-layer thin films deposited on Si substrates with a 1.1-μm-thick thermal oxide (SiO_2). VO_2 films with different thicknesses varying from 100 to 300 nm were prepared by pulsed laser deposition (PLD) (Figure 1c), and the majority of data shown in this work are based on an optimal VO_2 thickness of 118 ± 5 nm. Across the MIT, the as-deposited VO_2 film exhibits a drastic change in resistivity by over 2 orders of magnitude (Figure 1b), as well as a change in optical reflectivity under white light illumination. The Raman spectrum (Figure 1d) at room temperature shows strong peaks identified as the I phase of VO_2. These peaks decrease in intensity with increasing temperature and finally disappear due to metallicity of the high-temperature M phase.

SiO_2/Si is chosen as substrate because VO_2 films PLD deposited on the surface of amorphous SiO_2 are textured with the c_R axis lying in the plane of the substrate.[27] The structural texturing is the key that enables bimorph actuation based on VO_2; otherwise, a completely random orientation of micrograins in the VO_2 film would cause the c_R-axis shrinkage to be fully canceled by the expansion in a_R and b_R axes. In addition, the SiO_2 layer underneath VO_2 can be selectively removed with wet etch without damaging the VO_2 layer, thereby releasing the VO_2 film layer. Figure 2 shows the schematics of the microactuator fabrication process. Prior to the etching, Cr was lithographically patterned and deposited onto the VO_2 film by e-beam evaporation, and then rapidly thermal annealed at 150−300 °C for 120 s (Figure 2a and b). Cr is selected here because it wets VO_2 and has a high Young's modulus. Then a photoresist pattern was defined by photolithography to cover part of the substrate (Figure 2c), which later becomes the base part supporting the finally released actuator structures (see Figure S1 in the Supporting Information). Reactive ion etching (RIE) was used to etch the exposed parts of VO_2 without significant lateral etching (Figure 2d), and the parts of VO_2 protected by either Cr or photoresist remained unetched. Afterward, the substrate was immersed into buffered oxide etchant (BOE 5:1) for a period of time depending on the width of the pattern, so as to under-etch the SiO_2 layer beneath the Cr/VO_2 pattern. As a result, the Cr/VO_2 bimorph structures not protected by the photoresist were released from the substrate and became free-standing (Figure 2e). Finally, the BOE solution was gradually replaced by water and then acetone to dissolve the photoresist, followed by natural drying in air (Figure 2f). The fabrication process is able to make microactuator structures in batch with a wide variety of sizes and arbitrary geometries, as shown in the Supporting

dx.doi.org/10.1021/nl303405g | Nano Lett. 2012, 12, 6302−6308

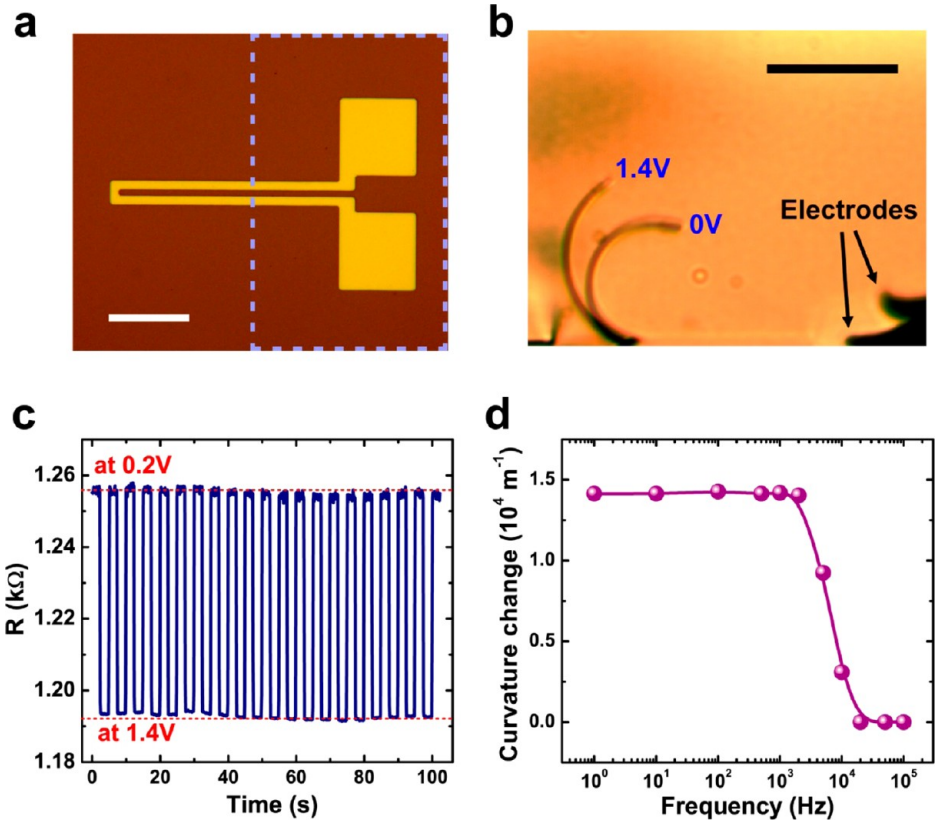

Figure 4. Electrically activated bimorph microactuators. (a) Top view of a microheater actuator patterned out of the Cr/VO_2 bimorph. The part outside the rectangular box will be under-etched and thus free-standing. The scale bar is 50 μm. (b) Side view of a microheater actuator activated by Joule heating. Bimorph is Cr/VO_2 = 50/118 nm. The scale bar is 50 μm. (c) Resistance of the actuator when a square wave of voltage is applied, showing a high durability of actuation. The voltage switches between 0.2 and 1.4 V at a frequency of 0.2 Hz. (d) Dependence of the bimorph curvature change on the frequency of the applied voltage, showing a half amplitude cutoff frequency (3 dB) of ~6 kHz.

Information (Figures S1 and S2). The released Cr/VO_2 bimorph curves toward the Cr side at room temperature. This is because the Cr was deposited onto VO_2 at a temperature higher than its MIT temperature when it was in the M phase with smaller in-plane lattice constants; as a result, when the Cr/VO_2 bimorph became free-standing at room temperature, the release of the built-in stress caused the bimorph to bend away from the VO_2 side.

The Cr/VO_2 bimorph exhibits a large change in curvature upon the MIT of the VO_2, acting as a thermally driven microactuator offering giant actuation amplitudes. Figure 3a shows side-view optical image of a cantilevered Cr/VO_2 bimorph at two temperatures merely 15 °C apart from each other across the MIT. The tip displacement for this 60-μm-long bimorph is 36 μm, giving a displacement (D)-to-length (L) ratio of D/L = 0.6. With a longer bimorph, a D/L exceeding 0.9 has been achieved (Figure S3). The high D/L is attributed to a giant change of ~22 000 m^{-1} in bimorph curvature across the MIT, as shown in Figure 3b, which mimics the MIT-induced resistivity change in Figure 1b. The curvature change is much higher than bimorphs based on other mechanisms such as differential thermal expansion and piezoelectricity; it is also higher than VO_2 film-coated Si cantilevers.[25,26] For such a bimorph with a rectangular cross section, the curvature change $\Delta\kappa = \Delta(1/R)$ is proportional to the relative length change (strain change $\Delta\varepsilon$) of the active layer (VO_2) in the bimorph,[28]

$$\Delta\kappa = \frac{6E_{Cr}E_{VO_2}t_{Cr}t_{VO_2}(t_{Cr}+t_{VO_2})}{E_{Cr}^2t_{Cr}^4 + 2E_{Cr}E_{VO_2}t_{Cr}t_{VO_2}(2t_{Cr}^2 + 3t_{Cr}t_{VO_2} + 2t_{VO_2}^2) + E_{VO_2}^2t_{VO_2}^4} \times \Delta\varepsilon \quad (1)$$

where E_{Cr} = 280 GPa and E_{VO_2} = 140 GPa are the Young's modulus of Cr and VO_2 layers, respectively, and t_{Cr} and t_{VO_2} are their thicknesses. Using this equation, an effective strain change of $\Delta\varepsilon \sim 0.3\%$ in VO_2 is estimated across the MIT. Although this is lower than the c_R-axis transformation strain (1%) in single-crystal VO_2, it is orders of magnitude higher than the strain deployed in existing bimorph actuators, namely, the strain caused by differential thermal expansion (estimated to be ~0.03% between VO_2 and Cr from 25 to 67 °C), and the strain accumulated in piezoelectric materials (typical ~0.01% at an applied field of 100 V/mm).

The relative actuation amplitude, represented by the tip displacement-to-length ratio D/L, is one of the key metrics for microscale actuation. Giant D/L allows actuators that occupy small volume to drive motion over long distance. Our giant D/L up to unity for L less than 100 μm is unusually large compared to other actuation techniques. As shown in Figure 3c, the D/L of all existing bimorph actuator technologies is limited to 0.4, despite their lengths exceeding 100 μm. We note that for a cantilever with given amount of change in bending curvature ($\Delta(1/R)$), its tip displacement D is proportional to the cantilever length L squared, instead of L (see Supporting Information, Figure S4). Therefore, a longer L favors not only higher D, but also higher D/L; thus achieving high D/L is

dx.doi.org/10.1021/nl303405g | Nano Lett. 2012, 12, 6302−6308

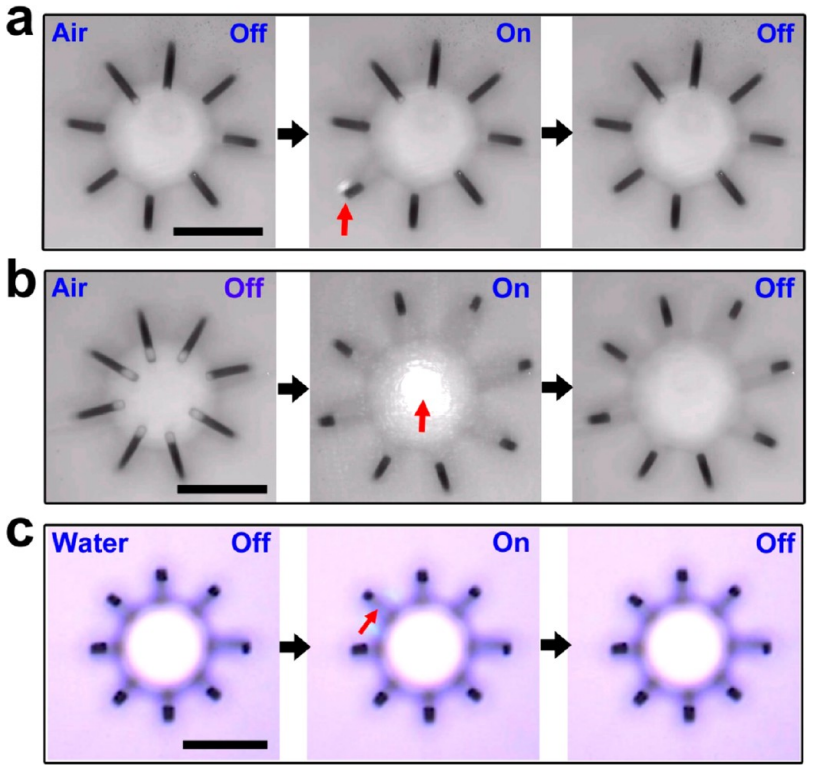

Figure 5. Optically activated bimorph microactuators, top view. (a) Activating one finger of the palm, and (b) the entire palm structure, with an incident laser. The laser power is 4 mW and substrate temperature is 25 °C (a) and 320 mW and 53 °C (b). Scale bars are 60 μm. (c) Actuating one finger in 40 °C water with a 5 mW laser. The scale bar is 50 μm. Red arrows indicate the laser spots. The total finger length is 100 μm (a and b) and 50 μm (c).

especially challenging for short L. Figure 3c shows that the Cr/VO_2 bimorph actuators provide the highest relative amplitude especially for the sub-100 μm regime. In addition, eq 1 indicates that the giant curvature change also benefits from the small thickness of the layers in the bimorph (100–200 nm), as $\Delta\kappa$ scales inversely with the thickness. In contrast, SMAs, the only other material competitive to VO_2 in terms of work density, cannot reach deep submicrometer thickness without sacrificing the actuation properties. We note that, for certain applications, thicker bimorphs may be needed to offer larger forces or higher work at the cost of actuation amplitude. Given the high Young's modulus and high work density of VO_2, a high force can be achieved at relatively small bimorph thicknesses. Effects of Cr thickness and annealing temperature on the actuation amplitude are shown and discussed in the Supporting Information (Figure S5).

The major advantages of the thin film based device fabrication are the size scalability and versatility in designing arbitrary patterns to fit different needs. Figure 3d shows a palm structure as a microactuator that can be thermally activated. Varying temperature from room temperature to 80 °C repeatedly opens and closes the palm (see Movie S1 in Supporting Information). Such a structure might be suitable for on-demand capturing and releasing micro-objects.

The actuation can be also activated electrothermally with an electric current or photothermally with a focused laser. Such electrical and optical control of the actuation offers capability of addressing individual devices at a much higher speed and smaller scale than by global heating. As shown in Figure 4a, a microheater structured actuator utilizes Joule heating of current flowing through the actuator itself to achieve the actuation. Owing to good electrical conductivity of the Cr and VO_2 layers, a small applied voltage (1.4 V) renders the actuator to bend at its maximum amplitude (Figure 4b) using a low input power of 1.6 mW. In ambient condition, the curvature changes by ~14 000 m^{-1} between the voltage ON and OFF states. The electrical actuation is also completely reversible free of materials fatigue and deterioration. Figure 4c shows the resistance of the actuator monitored during operation driven by an applied square-wave voltage alternating between 0.2 and 1.4 V at a frequency of 0.2 Hz. The resistance changes by 5% between the states under high and low voltages due to the current-controlled MIT of the VO_2 layer. The actuator went through tens of thousands of actuation cycles in air without noticeable degradation in performance, suggesting a long lifetime and high durability.

Figure 4d shows the dependence of curvature change on the frequency of the square-wave voltage applied. It can be seen that the actuation amplitude remains the same until the frequency exceeds 2 kHz (also see Movie S2). The 3 dB attenuation frequency (where the amplitude is reduced by half) is about 6 kHz, corresponding to a response time of ~0.17 ms. The actuation is completely cut off at ~20 kHz, where the pulsed heating becomes faster than the heat dissipation through thermal conduction to the substrate and convection to ambient air. This process is slower than piezoelectrically driven actuators (>tens of kHz), comparable to differential thermal expansion actuators, but much faster than shape memory alloy actuators and any polymer and ionic motion-based actuators (<hundreds of hertz).

Compared to thermal and electrical activation, photothermal activation by light is desired for contactless and spatially

dx.doi.org/10.1021/nl303405g | *Nano Lett.* 2012, 12, 6302–6308

resolved control of actuation. Figure 5 and Movie S3 show actuations of palm structures with a focused laser. The laser can address each finger of the palm individually at room temperature with a low power of ~4 mW (Figure 5a). This power value is on the order of, but larger than, the electrical Joule heating power required for the actuation (1.6 mW). This is partly because not all laser power is absorbed, and partly because the heating spot by the focused laser is more local with a higher temperature, thus causing a more severe heat dissipation. Light can also activate the entire palm structure globally (Figure 5b). Here, due to the limitation of the maximum laser power available, we elevated the substrate temperature to 53 °C so that the laser could heat the entire palm structure beyond the MIT temperature. We note that this base heating would be unnecessary if a more powerful laser is used, a black absorption layer is coated on the structure, or the palm structure is transferred to a thermally insulated substrate.

In addition to working in ambient air, the actuator also works well in aqueous environment. However, because water provides better heat sinking from the structure, higher light power or elevating the substrate temperature is required to heat the structure beyond the MIT temperature. Figure 5c shows a palm structure is soaked in de-ionized water heated at 40 °C. The actuation in water is stable, and the response speed is faster than 17 ms, the frame interval of the camera we used (Movie S3). This is much faster than other mechanisms currently used in aqueous actuation, such as hydrogel swelling and polymer electrostriction.[29,30] Therefore, properly designed Cr/VO_2 microactuators may be used for high-speed microfluidic valves/pumps and reversible molecular cargos in physiological environments.

In summary, VO_2-based bimorph microactuators with defined designs are fabricated in batch, which shows giant normalized amplitude over a small temperature rise, especially at the sub-100 μm length scale. The large normalized actuation amplitude (D/L) directly benefits from the giant strain across the phase transition, as well as the nanoscale thickness of the devices. Even if the length of the bimorph actuator scales down to 1 μm, its tip would still displace by more than 10 nm. Using the strain change of $\Delta\varepsilon$ = 0.3% observed in the VO_2 films in this work, a work density as high as 0.63 J/cm^3 is calculated. As a comparison, the work density would be ~0.001−0.01 J/cm^3 for the differential thermal expansion actuators (ΔT = 10 K) and typical piezoelectric actuators. Therefore, our microactuators offer not only large displacement, but also high work output; consequently, a high actuation force is expected without being compromised by the large displacement. The microfabrication process developed here is simple, versatile, scalable, and compatible with industry standards. The functionalities of actuation can be further enriched with integrated designs of planar as well as three-dimensional geometries. The diverse range of stimuli that the devices respond to greatly extends the speed and individual addressability of the microactuators. Taken together, a wide range of micro- and nanoscale applications can be envisioned where mechanical motion is needed at high displacement, high force, and high speed, such as micromanipulation, optomechanical and electromechanical switch, microfluidic valving and pumping, drug delivery, heat regulation, and artificial muscles.

■ ASSOCIATED CONTENT

Supporting Information

Experimental specifics, batch fabrication of microactuators, experimental data of tip displacement versus actuator length, geometry of bimorph, dependence of bimorph curvature on annealing temperature and Cr thickness, and videos showing thermal, electrical, and optical actuations for various microactuator structures. This material is available free of charge via the Internet at http://pubs.acs.org.

■ AUTHOR INFORMATION

Corresponding Author

*E-mail: wuj@berkeley.edu.

Notes

The authors declare no competing financial interest.

■ ACKNOWLEDGMENTS

This work was supported by the U.S. Department of Energy Early Career Award DE-FG02-11ER46796. The materials synthesis and theoretical analysis were supported by the National Science Foundation under Grant No. ECCS-1101779. Part of the device fabrication was done at the Lawrence Berkeley National Laboratory, which is supported by the Office of Science, Office of Basic Energy Sciences, of the U.S. Department of Energy under Contract No. DE-AC02-05CH11231.

■ REFERENCES

(1) Mirfakhrai, T.; Madden, J. D. W.; Baughman, R. H. *Mater. Today* **2007**, *10* (4), 30−38.
(2) Vaia, R.; Baur, J. *Science* **2008**, *319* (5862), 420−421.
(3) Koerner, H.; White, T. J.; Tabiryan, N. V.; Bunning, T. J.; Vaia, R. A. *Mater. Today* **2008**, *11* (7−8), 34−42.
(4) LeMieux, M. C.; McConney, M. E.; Lin, Y.-H.; Singamaneni, S.; Jiang, H.; Bunning, T. J.; Tsukruk, V. V. *Nano Lett.* **2006**, *6* (4), 730−734.
(5) Zheng, L.-S.; Lu, M. S.-C. *Sens. Actuators, A* **2007**, *136* (2), 697−703.
(6) Zhu, S.-E.; Shabani, R.; Rho, J.; Kim, Y.; Hong, B. H.; Ahn, J.-H.; Cho, H. J. *Nano Lett.* **2011**, *11* (3), 977−981.
(7) Steel, M. R.; Harrison, F.; Harper, P. G. *J. Phys. D: Appl. Phys.* **1978**, *11*, 979−989.
(8) King, T. G.; Preston, M. E.; Murphy, B. J. M.; Cannell, D. S. *Precis. Eng.* **1990**, *12*, 131−136.
(9) Wu, C. C. M.; Kahn, M.; Moy, W. *J. Am. Ceram. Soc.* **1996**, *79*, 809−812.
(10) Wood, R. J.; Steltz, E.; Fearing, R. S. *Sens. Actuators, A* **2005**, *119* (2), 476−488.
(11) Krulevitch, P.; Lee, A. P.; Ramsey, P. B.; Trevino, J. C.; Hamilton, J.; Northp, M. A. *J. Microelectromech. Sys.* **1996**, *5*, 270−282.
(12) Makino, E.; Mineta, T.; Mitsunaga, T.; Kawashima, T.; Shibata, T. *Microelectron. Eng.* **2011**, *88* (8), 2662−2665.
(13) Baughman, R. H.; Cui, C.; Zakhidov, A. A.; Iqbal, Z.; Barisci, J. N.; Spinks, G. M.; Wallace, G. G.; Mazzoldi, A.; Rossi, D. D.; Rinzler, A. G.; Jaschinski, O.; Roth, S.; Kertesz, M. *Science* **1999**, *284* (5418), 1340−1344.
(14) Landi, B. J.; Raffaelle, R. P.; Heben, M. J.; Alleman, J. L.; VanDerveer, W.; Gennett, T. *Nano Lett.* **2002**, *2* (11), 1329−1332.
(15) Chen, L.; Liu, C.; Liu, K.; Meng, C.; Hu, C.; Wang, J.; Fan, S. *ACS Nano* **2011**, *5* (3), 1588−1593.
(16) Li, J.; Ma, W.; Song, L.; Niu, Z.; Cai, L.; Zeng, Q.; Zhang, X.; Dong, H.; Zhao, D.; Zhou, W.; Xie, S. *Nano Lett.* **2011**, *11* (11), 4636−4641.

(17) Zhang, X.; Pint, C. L.; Lee, M. H.; Schubert, B. E.; Jamshidi, A.; Takei, K.; Ko, H.; Gillies, A.; Bardhan, R.; Urban, J. J.; Wu, M.; Fearing, R.; Javey, A. *Nano Lett.* **2011**, *11* (8), 3239−3244.
(18) Huber, J. E.; Fleck, N. A.; Ashby, M. F. *Proc. Math. Phys. Eng. Sci.* **1997**, *453*, 2185−2205.
(19) Zhang, Q. M.; Bharti, V.; Zhao, X. *Science* **1998**, *280*, 2101−2104.
(20) Wu, J.; Gu, Q.; Guiton, B. S.; de Leon, N. P.; Ouyang, L.; Park, H. *Nano Lett.* **2006**, *6*, 2313−2317.
(21) Cao, J.; Ertekin, E.; Srinivasan, V.; Fan, W.; Huang, S.; Zheng, H.; Yim, J. W. L.; Khanal, D. R.; Ogletree, D. F.; Grossman, J. C.; Wu, J. *Nat. Nanotechnol.* **2009**, *4*, 732−737.
(22) Wei, J.; Wang, Z.; Chen, W.; Cobden, D. H. *Nat. Nanotechnol.* **2009**, *4*, 420−424.
(23) Wall, S.; Wegkamp, D.; Foglia, L.; Appavoo, K.; Nag, J.; Haglund, R. F., Jr.; Stähler, J.; Wolf, M. *Nat. Commun.* **2012**, *3*, 721.
(24) Cao, J.; Fan, W.; Zhou, Q.; Sheu, E.; Liu, A.; Barrett, C.; Wu, J. *J. Appl. Phys.* **2010**, *108* (8), 083538.
(25) Rúa, A.; Fernández, F. E.; Sepúlveda, N. *J. Appl. Phys.* **2010**, *107* (7), 074506.
(26) Cabrera, R.; Merced, E.; Sepúlveda, N.; Fernández, F. E. *J. Appl. Phys.* **2011**, *110* (9), 094510.
(27) Rivera, F.; Burk, L.; Davis, R.; Vanfleet, R. *Thin Solid Films* **2012**, *520* (7), 2461−2466.
(28) Timoshenko, S. *J. Opt. Soc. Am.* **1925**, *11*, 233−255.
(29) Sershen, S. R.; Mensing, G. A.; Ng, M.; Halas, N. J.; Beebe, D. J.; West, J. L. *Adv. Mater.* **2005**, *17*, 1366−1368.
(30) Garcia-Cordero, J. L.; Kurzbuch, D.; Benito-Lopez, F.; Diamond, D.; Lee, L. P.; Ricco, A. J. *Lab Chip* **2010**, *10* (20), 2680−2687.